The distribution of motional correlation times in superionic conductors: ^{19}F nuclear magnetic resonance of tysonite-like LaF_3

1997 J. Phys.: Condens. Matter 9 9275

(http://iopscience.iop.org/0953-8984/9/43/012)

J. Phys.: Condens. Matter **9** (1997) 9275–9287. Printed in the UK PII: S0953-8984(97)82693-8

The distribution of motional correlation times in superionic conductors: ^{19}F nuclear magnetic resonance of tysonite-like LaF_3

A F Privalov†, A Cenian‡¶, F Fujara§, H Gabriel‡, I V Murin‖ and H-M Vieth†

† Institut für Experimentalphysik, Freie Universität Berlin, Arnimallee 14, D-14195 Berlin, Germany

‡ Institut für Theoretische Physik, Freie Universität Berlin, Arnimallee 14, D-14195 Berlin, Germany

§ Fachbereich Physik, Universität Dortmund, D-44221 Dortmund, Germany

‖ Chemical Department of St Petersburg State University, Universitetskij Prospekt 2, Petrodvoretz, 198904, St Petersburg, Russia

Received 18 March 1997

Abstract. Fluorine mobility at different structural positions in monocrystalline LaF_3 with the tysonite structure is analysed using ^{19}F NMR line-shape analysis. The method is sensitive to ionic exchange with correlation times in the range 10^{-6}–10^{-3} s. For the temperature range between 240 K and 400 K the motion is restricted mainly to the F^- ions in the fluorine layers perpendicular to the main symmetry axis (the F_1 sublattice), while F^- ions in the La plane ($F_{2,3}$) remain immobile. No significant anisotropy of the F_1-ionic diffusion within the layers and along the c-axis is found ($D_{\|c} \approx D_{\perp c} \approx 6 \times 10^{-14}$ m^2 s^{-1} at 400 K). From NMR spectra it is clear that F_1 mobility is strongly heterogeneous. The motional disorder can be described well by a broad distribution of correlation times, $G(\tau)$, which has a shape close to a log–Gaussian function and reflects the potential energy landscape in the superionic state. The variation of the centre position and width of $G(\tau)$ with temperature differs from an Arrhenius law behaviour. Ionic mobility on the microscopical scale, therefore, cannot be considered a process which is activated only thermally. Applying MD techniques shows that the presence of vacancies may lead to pronounced changes of the potential energies, and supports the idea that there is a distribution of activation energies.

1. Introduction

For the origin of the superionic state in superionic conductors (SICs), usually motional disorder in one of the ionic sublattices is seen to be responsible [1]. Nevertheless, the standard analysis of ionic motion in SICs is based on the assumption of a thermally activated Arrhenius-like process with a single activation energy and one average motional correlation time. Such an approach excludes disorder from consideration and can therefore not be used to gain any information on the existing motional heterogeneity in the superionic state.

Analysis of motional heterogeneity is common for various disordered systems [2], but for disorder in superionic solids experimental evidence is rare because only few methods are sensitive to it.

¶ Permanent address: Institute of Fluid Flow Machines, Polish Academy of Science, 80-952 Gdansk, Ulica Fiszera 14, Poland.

0953-8984/97/439275+13$19.50

One of them is the analysis of NMR spin–lattice relaxation times T_1. In several superionic conductors the standard Bloembergen–Purcell–Pound (BPP) model of relaxation fails, when a single correlation time is assumed. This is demonstrated by the following features: the $\ln T_1$ versus $1/T$ plot is not symmetrical with respect to the temperature at which the T_1-minimum occurs. Furthermore, for the low-temperature branch the proportionality $T_1 \propto \omega^2$ is violated [3, 4]. To describe these observations, an analysis was suggested which takes a distribution of activation energies into account [4]. Likewise, measurements of spin–lattice relaxation of ^{23}Na in β-alumina showing a highly asymmetric $\ln T_1$ versus $1/T$ minimum were analysed assuming a distribution of activation energies [5]. In the glassy SIC $0.56Li_2S + 0.44SiS_2$ the deviation from BPP behaviour as well as the anomalous conductivity $\sigma(\omega)$ were explained satisfactorily by a model of lithium-ion motion with a Gaussian distribution of activation energies [6]. In a similar way experimental data on dielectrical relaxation spectroscopy in superionic materials were successfully modelled using a distribution of correlation times and activation energies [7]. For the case of frequency-dependent conductivity in SIC glass it was shown that the use of a distribution of activation energies, even a very simple, rectangular one, is able to improve significantly the fit to the experimental data [8]. In the jump relaxation model, developed to describe dynamical processes in SICs, a scheme of double potential wells is used with a distribution of the potential barriers [9]. A distribution of activation energies with a log–Gaussian shape has been used to explain ^{7}Li NMR spin–lattice relaxation and ionic conductivity in the glassy system $xLi_2S + (1-x)GeS_2$ [10].

Most investigations of motional heterogeneity have been performed on glassy SICs, where the motional disorder is stimulated by a structural disorder. But even in such cases of strong heterogeneity the shape of the distribution function was not measured directly, but was taken from a fit to a model function. The actual observables, such as T_1 or σ, are in general not very sensitive to the shape of the model function and thus give only qualitative information. In crystalline SICs, where a part of the sublattices keeps an ordered structure, a much less pronounced motional heterogeneity is expected and for any reliable information one has to concentrate on methods which are particularly sensitive to disorder.

Since the NMR observables reflect the local environment of spins, this technique is well suited to the study of disordered systems. The line shape resulting from dipolar spin coupling and from chemical shifts is very sensitive to the spin mobility. From ^{19}F NMR line-shape studies one can gain information on ionic motion with correlation times in the range of 10^{-6}–10^{-3} s. Fluorine NMR has the advantages of high sensitivity and of large chemical shifts allowing one to resolve spectral contributions from different structural sites. For this reason we applied ^{19}F NMR for the analysis of the heterogeneity of ionic exchange in lanthanum fluoride with the tysonite structure. This substance is known as a typical superionic conductor in which the fluoride anions transport the electric charges.

Lanthanum fluoride possesses trigonal structure ($P\bar{3}c1$) where the La^{3+} cations are located in planes perpendicular to the main symmetry axis (the c-axis) [11–13]. The La^{3+} cations remain immobile up to the melting point of about 1770 K. The fluorine anions are located at three distinct structural sites, F_1, F_2 and F_3, in the ratio of 12:4:2 per unit cell. Two sublattices, F_2 and F_3, are structurally and dynamically nearly identical and can be considered as one common $F_{2,3}$ sublattice, at least with respect to NMR experiments [14]. The fluorine ions are not only structurally but also dynamically inequivalent. The ionic transport properties of LaF_3 have been investigated for many years by various techniques [14–23]. It is assumed that ionic mobility is caused by disorder in one of the fluorine sublattices and initiated by the formation of F^- vacancies [15]. Interstitial Frenkel-type defects are too rare to significantly affect the mobility at temperatures below 1000 K

[16]. From ^{19}F NMR data obtained at high external field it became evident that for temperatures below 400 K the disordering and ionic motion takes place mainly within the F_1 sublattice [23].

In this paper we discuss the ionic mobility in single crystals of LaF_3 at temperatures ranging from 130 K to 400 K. We focus on the motion in the F_1 sublattice and especially on the characterization of disorder in this process.

2. Experimental procedure

In the solid state, ^{19}F NMR spectra are usually dominated by contributions from dipolar spin coupling and chemical shifts (CS). In general it is difficult to correctly record the contributions from the two interactions together. With the spin–echo techniques it is not possible to refocus the two interactions simultaneously: the solid echo cannot fully refocus chemical shifts, while the Hahn echo has problems with refocusing dipole–dipole interactions. The free-induction decay, because of spectrometer dead time, can be recorded only with a finite delay after the rf excitation pulse causing spectral distortions. In our case the latter method gave the best results; accordingly our ^{19}F NMR spectra are Fourier transforms of the free-induction decays recorded at an external field of 7.05 T corresponding to a resonance frequency of 282 MHz. The length of the 90° rf excitation pulse is 1 μs, which is sufficiently short for exciting the necessary spectral range. The dead time in our experiment is around 2.5 μs.

For the measurements of the diffusion coefficients D a different technique was used. The transversal spin relaxation caused by ionic motion in a strong static magnetic field gradient ($g = 180$ T m^{-1}) was measured at 90 MHz [24]. This technique yields directly values for D, without one making particular model assumptions for the motion. We applied it also to measure the anisotropy of the diffusion. Because the largest principal component of the gradient tensor is parallel to the B_0-direction, and all other components can be neglected, only the spin motion in this direction is observed. By proper orientation of the crystal in the magnetic field the diffusion coefficients have been measured parallel ($D_\parallel$) and perpendicular ($D_\perp$) to the crystalline c-axis, the main symmetry axis of the tysonite structure.

The sample used is a rectangular single crystal of LaF_3 with the dimensions $3 \times 3 \times 7$ mm^3. Its quality was checked optically and the direction of its c-axis was determined using the Laue x-ray diffraction method. The sample was oriented with respect to the external magnetic field with an accuracy of 2°. The temperature in the range 130 K–400 K was set with an accuracy of 1 K and stabilized to ± 0.1 K.

3. Results and analysis

In figure 1, ^{19}F NMR spectra of monocrystalline LaF_3 with $\boldsymbol{B}_0$ oriented along the c-axis are shown for a set of different temperatures. Each spectrum consists of two components with an intensity ratio around 2:1 and chemical shifts of -64 ppm and 105 ppm with respect to $CFCl_3$ as the reference. As mentioned above, the F_2 and F_3 ions give an almost identical NMR line and to a good approximation they can be described as one common $F_{2,3}$ sublattice [23]. The low-intensity spectral component is from the $F_{2,3}$ and the high-intensity line is from the F_1 sublattice. The chemical shift for both spectral components is anisotropic and the largest splitting between the two lines is observed when the crystal is oriented with $\boldsymbol{B}_0 \| \boldsymbol{c}$. This orientation has been used for the analysis for the following reasons: the F_1 and $F_{2,3}$ components can be observed separately and the additional doublet splitting of the F_1

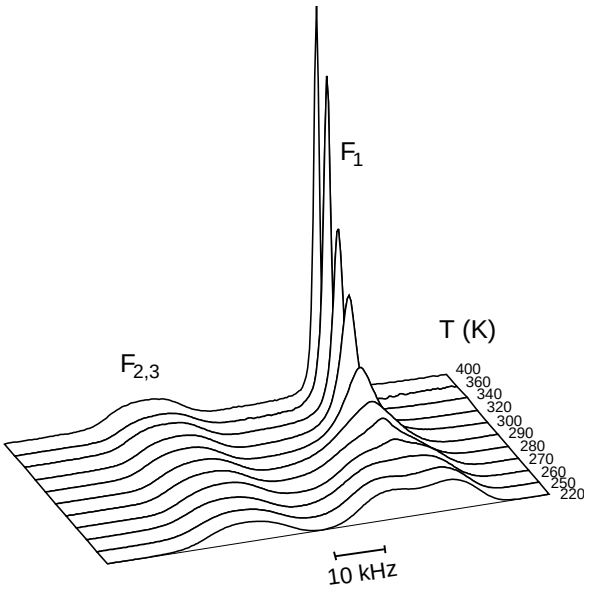

Figure 1. Experimental ^{19}F spectra of monocrystalline LaF_3 for $\boldsymbol{B}_0 \| c$-axis.

component at this orientation increases the dynamical range of the motional analysis. In the temperature range below 250 K the spectrum does not undergo any visible changes. The signal from the F_1 sublattice shows a partially resolved dipolar structure with a splitting of about 17 kHz. From model calculations (see below) one can see that only motion with correlation times $\tau < 200$ μs is able to affect the F_1 line shape; hence, we can conclude that below 250 K ionic exchange is slower. With increasing temperature, substantial ionic motion begins in the F_1 sublattice as inferred from the loss of the doublet structure and the motional narrowing of this line. In contrast, the $F_{2,3}$ line does not show any detectable changes up to temperatures around 400 K. Also, the centre position of each of the two spectral components stays unchanged below 400 K. From this we conclude that the $F_{2,3}$ ions are not involved in any motional process with $\tau < 1$ ms. It is remarkable that the high mobility in the F_1 sublattice does not affect the dipolar broadening of the $F_{2,3}$ component. This is due to the comparatively small dipolar coupling between F_1 and $F_{2,3}$ ions.

Since significant ionic motion at temperatures below 400 K is detected only for the F_1 ions, we will focus in the rest of this paper on the detailed analysis of the dynamical processes on this sublattice.

3.1. Determination of the ionic jump anisotropy

For the numerical model calculation of the dynamical NMR line shape one has to estimate realistic parameters for the ionic exchange process. In particular the rates for jumps in different directions have to be assessed. To evaluate such jump rates, knowledge of the ionic distances, and of the heights and profiles of interatomic lattice potentials is required. The distances are known from x-ray analysis, but the potentials are not known. Nevertheless, the ratio of the correlation times of ionic jumps along different paths has been estimated from the anisotropic diffusion coefficient data in the following way.

In tysonite, where the number of inequivalent jumps is large, a significant simplification

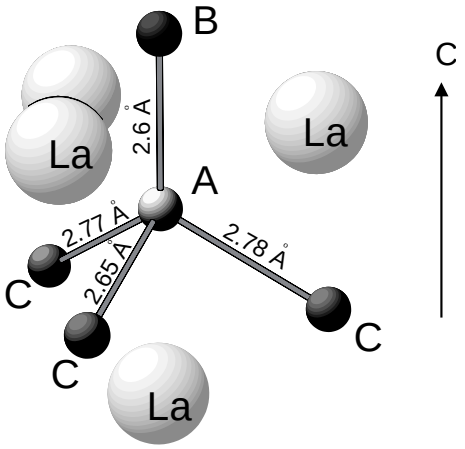

Figure 2. Pathways of the jumping ion (denoted as A) in the F_1 sublattice (see the text).

can be made by restricting the motion to exchange among F_1 sites. The set of nearest-neighbour sites in the F_1 sublattice is shown in figure 2. The F_1 ion marked as A is surrounded by four adjacent F_1 sites. One, denoted by B, is located at an angle $\Theta_1 = 17.4^\circ$ with respect to the c-direction and at a distance $r_1 = 2.6$ Å from A. The other three, all denoted by C, are sitting at almost equivalent sites at an angle $\Theta_2 = 116^\circ$ and a distance $r_1 = 2.65$–2.78 Å. Therefore we distinguish only between two different jumps, jump A $\longrightarrow$ B with the rate ν_1 and A $\longrightarrow$ C with the rate ν_2. They give rise to diffusive flow with the coefficient $D_\parallel$ parallel to the c-direction and with the coefficient $D_\perp$ perpendicular to it. Taking this local geometrical arrangement, one obtains that $\nu_1/\nu_2 \approx D_\parallel/D_\perp$. In the T_2-relaxation measurements at high magnetic field gradient as described above, no substantial anisotropy of the diffusion was found; $D_\parallel \approx D_\perp \approx (6 \pm 1) \times 10^{-14}$ m^2 s^{-1} for the F_1 ions at 400 K. At this temperature the conductivity measurements on LaF_3 also show no sign of any significant anisotropy of the fluorine conductivity [18]. Even when allowing for larger uncertainties in the experimental determination of D and in the evaluation of exchange rates, there is no reason to assume that ionic jumps along different directions in the F_1 sublattice take place at substantially different rates.

3.2. Calculation of the NMR line shape

In solid-state ^{19}F NMR, the spectral shape is dominated by magnetic dipole interactions and chemical shifts. Because the strongest dipole–dipole interactions among the F_1 ions (about 17 kHz) are significantly lower than the difference of the chemical shift between the F_1 and the $F_{2,3}$ ions and higher than the dipolar coupling between the F_1 and the $F_{2,3}$ ions (about 3.6 kHz), we can analyse ionic motion on the F_1 sublattice separately.

Since an exact calculation of NMR spectra in solids is in general impossible due to the enormous number of interacting spins, we used the following approximation for the dipolar coupling [23]. First the line shape for the rigid structure was calculated for $\boldsymbol{B}_0 \| \boldsymbol{c}$. The ionic positions were taken from x-ray data. Because for this orientation all spins on each individual sublattice are equivalent, their NMR spectra are identical and the problem can be simplified to the case of a single spin which interacts with its neighbouring spins. The dipole–dipole spin coupling decreases with distance r as r^{-3} and thus only nearest

neighbours contribute significantly to the splitting of the energy levels. The dipole–dipole interactions among N such neighbours result in 2^N spectral components. To model the experimental NMR line shape, dipolar couplings with distant spins are taken into account by convolution of the spectral components with a Gaussian broadening function. The number N_n of near neighbours necessary for arriving at a stable line shape was determined empirically in several test runs. We found, that an increase of N_n beyond 5 does not lead to any noticeable changes in the line shape. This number was used for the calculation of all NMR spectra.

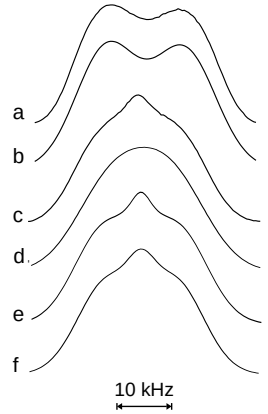

Figure 3. ^{19}F NMR spectra for the F_1 sublattice: (a) experimental, at 220 K; (b) the calculated dipolar spectrum for the rigid structure; (c) experimental, at 270 K; (d) calculated, with one correlation time $\tau = 35$ μs; (e) calculated, with two correlation times, $\tau_f = 4$ μs, $\tau_s = 45$ μs, and the intensity ratio $N_f/N_s = 0.12$; (f) reconstructed after equation (2), with the log–Gaussian function $G(\tau)$ after equation (3), with $\tau^c = 30$ μs and $\delta = 0.8$.

The influence of a spin diffusion has to be considered if NMR spectral analysis is used to gain dynamical information. In the case of fluorine exchange among F_1 sites in LaF_3 we estimated the spin diffusion to be slow in comparison with the motional ionic exchange giving rise to the change in line shape. Even the experimental spectrum for the F_1 ions in the rigid limit ($T < 250$ K; see figure 3(a)) which is expected to show the strongest influence of spin diffusion can be well approximated without taking into account spin diffusion (figure 3(b)). Since spin diffusion commonly shows hardly any change with temperature we neglected it for all of our measurements.

For the analysis of dynamical processes on the F_1 sublattice the line shape was numerically simulated by taking into account ionic exchange among the same five sites. Assuming that ionic exchange is induced by the presence of vacancies implies that only ions in the immediate neighbourhood of an empty site will participate in the exchange process. The concentration of vacancies is low and hence most of the time each microvolume of five sites stays unchanged. The correlation time relevant for the NMR features corresponds to the average lifetime of such a spin configuration. For the model calculations we solved the standard stochastic Liouville equation for the spin-density matrix with an additive term to describe the evolution of the spin ensemble under the condition of motional exchange [25].

First a simple motional process with a single rate τ describing the ionic exchange was considered. The simulated spectra for F_1 ions at various correlation times are shown in figure 4. Comparison shows that the experimental spectra can only be approximated unsatisfactorily by the simulations. For example, the experimental spectrum obtained at

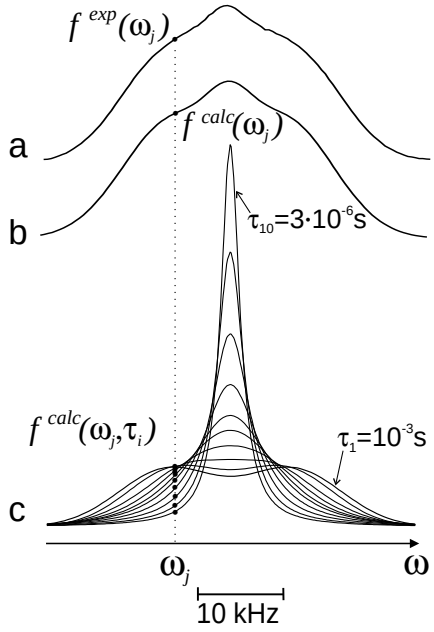

Figure 4. (a) The experimental line shape $f^{exp}(\omega)$ for the F_1 sublattice, (b) the calculated line shape $f^{calc}(\omega)$, and (c) the set of calculated line shapes $f^{calc}(\omega, \tau_i)$ for 3×10^{-6} s $\leqslant \tau_i \leqslant 10^{-3}$ s.

270 K (figure 3(c)) shows an intense narrow component in the central part that is not reproduced in the corresponding simulation (figure 3(d)) calculated with $\tau = 35$ μs as the best fit for the ionic exchange at this temperature. This spectral feature can however be explained if one superimposes contributions from ions undergoing rather fast exchange with contributions from slowly exchanging spins.

3.3. Analysis of the motional heterogeneity

In comparison with the timescales of other standard analytical methods such as x-ray or neutron scattering, the characteristic timescale of NMR is much longer. For resolving the relevant spectral features an NMR signal acquisition time of several hundred microseconds is necessary. Heterogeneities can only be observed to the extent that they are not averaged on this timescale. Motional heterogeneity, in particular, can only be seen if the spatial fluctuations of the interionic potential have a sufficiently long range in comparison with the typical distances which the ions cross during the NMR time window. A simple estimate of the fluctuation length of the potential, assuming a motional correlation time of 35 μs (270 K), an NMR window of 100 μs, and interionic distances of 2.7 Å, gives a size comparable with the dimensions of the crystalline unit cell. On increasing the temperature, the ions become more mobile; hence the relevant path length becomes longer and eventually comparable with the fluctuation length, thus causing the disappearance of inhomogeneity effects.

To describe the motional inhomogeneity on the F_1 sublattice we have compared two modified models. The first one uses two distinct correlation times τ_f and τ_s (the labels f and s refer to fast and slow, respectively). We consider these together with the ratio of the corresponding number of spins N_f/N_s, and thus have a three-parameter model, which provides significantly better fits to the experimental data than the model with a single

correlation time referred to in the previous section. The best fit to the experimental line shape is shown in figure 3(e); it was obtained for $\tau_f = 4\ \mu$s, $\tau_s = 45\ \mu$s and $N_f/N_s = 0.12$. Apparently, there is no physical description of the system on the basis of which the large difference in the values of the correlations can be explained.

Our second approach is based on the assumption that a larger set of correlation times exists, which will be described by a continuous distribution function $G(\tau)$. It rests on the idea that the ions on the real F_1 sublattice are located in different local environments with differing potential energy surfaces. The resulting spread in the mobilities corresponds to a temperature-dependent distribution of correlation times $G(\tau)$ that is determined as follows. We choose a finite set of correlation times τ_i $(i = 1, 2, \ldots, n)$ within a physically reasonable time range, say 10^{-6} s $\leqslant \tau_i \leqslant 10^{-3}$ s, in our case. It is used to calculate the line shape $f^{calc}(\omega, \tau_i)$ for each τ_i by using the procedure described in section 3.2. Figure 4(c) collects the results of such calculations for ten different correlation times within the range just specified. A resulting line shape $f^{calc}(\omega)$ (an example is given in figure 4(b)) is then defined as a weighted superposition of the individual line shapes $f^{calc}(\omega, \tau_i)$:

$$f^{calc}(\omega) = \sum_{i=1}^{n} p_i f^{calc}(\omega, \tau_i). \tag{1}$$

The unknown weight factors p_i are determined by demanding $f^{calc}(\omega)$ to become the best approximation to the experimental line shape $f^{exp}(\omega)$ shown in figure 4(a).

The experimental spectrum $f^{exp}(\omega)$ is recorded with noise and phase correction artifacts. It results from a digital Fourier transform as a set of discrete amplitudes obtained numerically. For this reason the function $f^{exp}(\omega)$ is represented by a discrete set of values $f^{exp}(\omega_j)$ at a sufficiently large number m of frequencies ω_j. The requirement $f^{calc}(\omega) = f^{exp}(\omega)$ leads to a system of inhomogeneous linear equations of dimension $m \times n$ (see figure 4):

$$f^{exp}(\omega_j) = \sum_{i=1}^{n} p_i f_i(\omega_j, \tau_i) \qquad (j = 1, 2, \ldots, m). \tag{2}$$

The overdetermined system (2) is solved numerically for the weight factors p_i by using a regularization procedure described e.g. in reference [26] to minimize the effects of the artifacts inherent in $f^{exp}(\omega)$.

The resulting discrete set of p_i-values (obtained for $n = 20$ and $m = 40$), is shown in figure 5 for various temperatures. Apparently, the corresponding continuous distribution function $G(\tau)$ (not drawn in figure 5) can be approximated well by a log–Gaussian function:

$$G(\log(\tau)) = A \exp\left(-\frac{1}{2}\left(\frac{\log(\tau/\tau^c)}{\delta}\right)^2\right) \tag{3}$$

which carries only two fitting parameters, the centre position τ^c and the width $\delta = (1/2)\log(\Delta_2/\Delta_1)$ where Δ_1 and Δ_2 are the points of maximal slope of $G(\log(\tau))$. This is illustrated by the full lines in figure 5. The model function (3) allows us to redefine the relative populations p_i for the individual discrete correlation times τ_i and to use them to get the line shape after solution of the system (2). By comparison of the calculated line shape with the experimental one, both parameters are adjusted to get the best fit. Because only two fitting parameters are used, they can be determined with good accuracy, especially in the presence of noise and artifacts from the spectral corrections. On the other hand, however, details in the shape of the real distribution function cannot be resolved.

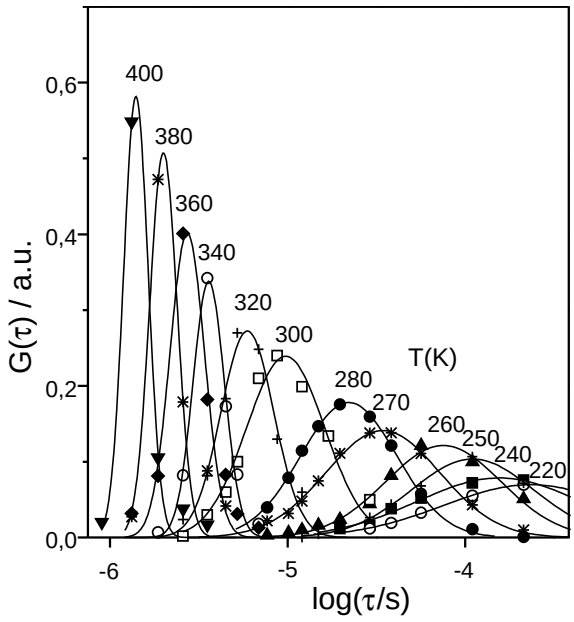

Figure 5. The distribution $G(\tau)$ of correlation times for F_1 ions at various temperatures. The lines show the best log–Gaussian fits.

Table 1. Comparison of the standard deviation of fits using one correlation time (figure 3(d)), two correlation times (figure 3(e)) and a distribution of correlation times (figure 3(f)) from the experimental spectrum (figure 3(c)).

Model	One τ	Two τ	Distribution $G(\tau)$
Fitting parameter	$\tau = 35\ \mu$s	$\tau_1 = 4\ \mu$s $\tau_2 = 45\ \mu$s $N_f/N_s = 0.12$	$\tau^c = 30\ \mu$s $\delta = 0.8$
Standard deviation	0.82	0.13	0.04

As an example, figure 3(f) displays the spectrum reconstructed with the resulting $G(\tau)$ for 270 K. The best fit is obtained for $\tau^c = 30\ \mu$s and $\delta = 0.8$. Based on a standard least-squares procedure, a comparison of the fit accuracy of the three above-described models is given in table 1. The best fit to the experimental results is obviously obtained using the model with a distribution of correlation times.

Notice that the numerical determination of the weight factors p_i supports the idea of a correlation time distribution. If only two correlation times, a fast and a slow one, were present, the solution of equation (2) would give two distinct components, in clear contradiction to our results.

We consider such a distribution of correlation times a more adequate description also from the physical point of view. A distribution of vacancies in a superionic conductor causes a distribution of the potential barriers and under the assumption of thermally activated processes will lead to a distribution $G(\tau)$ of correlation times. (A further discussion will be given below.) The temperature dependence of the optimal τ^c- and δ-values from the fit based on equation (3) is shown in figure 6. With increasing temperature, the centre of

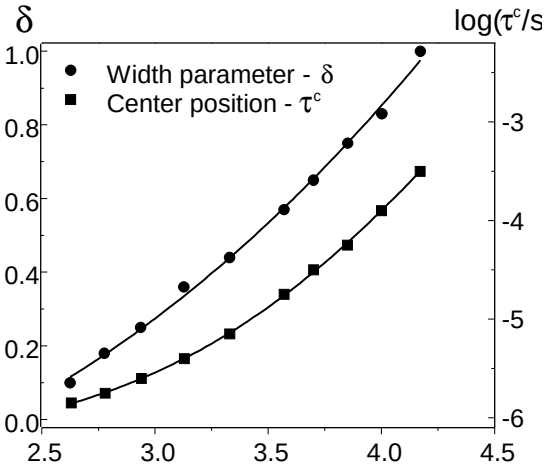

Figure 6. The centre and width parameters of the Gaussian fit for the distribution $G(\log(\tau))$.

the distribution shifts to shorter correlation times and the distribution becomes narrower, as expected for an activated process. For the case of thermal activation with an Arrhenius law behaviour:

$$\tau = \tau_0 \exp(E_a/kT) \tag{4}$$

the distribution of correlation times transforms into a distribution of potential barriers for the ionic motion. In this case the width δ and the centre position τ^c of $G(\tau)$ are linear functions of the inverse temperature $1/T$. The results of our analysis shown in figure 6 exhibit significant deviations from such a linear behaviour. One can conclude that ionic mobility is not a simple thermally activated process. A similar behaviour has been found for various disordered systems [27]. However, such a result for lanthanum fluoride is in disagreement with conductivity data, where a linear Arrhenius-like behaviour of σ was found for temperatures up to 400 K [15, 18]. Only the linear low-temperature part of the plot in figure 6 has the same slope as the one found in the conductivity measurements. Since the NMR observables are particularly sensitive to processes on the microscopic scale, one can conclude that on this short range additional factors have to be taken into account if one is to understand the ionic motion.

3.4. The origin of a distribution of activation energies—a simple model

To check whether a distribution of activation energies for the migration of F atoms can be traced to the presence of adjacent vacancies, we have performed the following model calculation. We consider a rigid LaF_3 lattice consisting of 34 056 atoms placed in their equilibrium positions. This amounts to 1419 unit cells arranged in increasing order with respect to a central box. The elementary cell (consisting of 6 La and 18 F atoms, respectively) was adopted to ensure both charge neutrality and vanishing dipole moment. The crystal structure was built up with the help of the atomic parameters given in reference [12] and it was checked that it gives the proper distances between the various shell atoms [11]. The potential that was used includes a repulsive Buckingham term:

$$V_r = A \exp(-r_{ij}/\rho_{i,j}) - C_{ij}/r_{ij}^6 \tag{5}$$

and a Madelung term:

$$V_m = q_i q_j / r_{ij} \tag{6}$$

and also the polarization energy

$$U_p = -(1/2)\alpha_i E^2(r_i). \tag{7}$$

$\boldsymbol{E}(r_i)$ is the electric field seen by the ith atom, and α_i is the atomic polarizability according to the shell model of Dick and Overhauser expressed in terms of shell charges Y and spring constant k ($\alpha = Y^2/k$). The potential parameters are taken from reference [16].

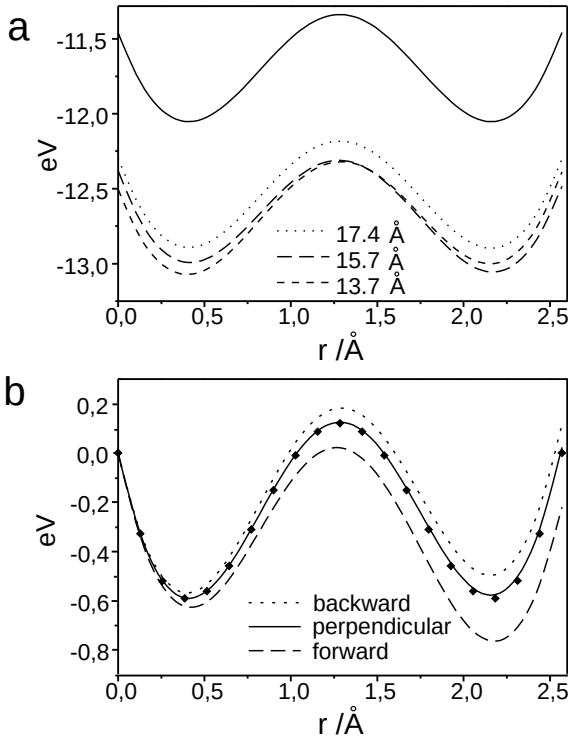

Figure 7. Potential energies as a function of the distance from a centre F_1 in the direction of a vacancy at the nearest F_1 position. (a) Solid curve: a single vacancy. Broken curves: an additional second F_1 vacancy at various distances. (b) A second F_1 vacancy at a fixed distance (13.7 Å) in different positions with respect to the F_1–F_1 direction; all of the energies were set equal to zero at $r = 0$, the F_1-centre position in the unrelaxed crystal. The diamonds represent the single-vacancy case.

After having generated the perfect lattice we produce a single vacancy at various crystallographic sites and look for its effect on the energy barriers 'seen' by F_1 atoms in a jump process to the adjacent F_1 vacancy. In the present preliminary estimation, relaxation of the lattice is not taken into account. The solid curve in figure 7(a) shows the potential as a function of the distance from the F_1 atom in the direction towards a single vacancy located at the next-nearest F_1 site (2.568 Å away). The three lower curves display the potential change when an additional second vacancy is placed at distances 13.7, 15.7 and 17.4 Å, respectively. The latter represent the average distances between the vacancies at concentrations defined with respect to the total number of fluorine atoms, equal to 0.17, 0.11 and 0.083%, respectively. The experimental study was performed at an

estimated concentration of 0.1%. Two minima occur in all of the curves, indicating that due to vacancy production atoms residing at sites of the originally perfect lattice experience forces. The resulting relaxation process shifts the F atom towards the vacancy because of the reduced Coulomb repulsion. The situation is completely symmetric in the presence of a single vacancy, i.e. after the jump, F_1 will have its equilibrium position near the newly formed vacancy (in its old position) and not at 2.568 Å. The presence of these minima in the unrelaxed crystal suggests introducing an effective activation barrier E_b defined as the difference between the maximum and the value of the potential energy at $r = 0$. In the case in which only a single vacancy is present, we find $E_b = 112$ meV, which is small compared to 711 meV, the difference of the potential maximum and minimum.

On placing the second vacancy at the distances given above, the energies shift to larger negative values as a result of a further lack of repulsive interaction. We now find E_b equal to 183, 68 and 112 meV when the second defect is at distances of 13.7, 15.7 and 17.4 Å, respectively. Notice that either an increase or a decrease of E_b can occur. The size of the barrier shift depends on the mutual separation of the two vacancies, but more strongly on the location of the second defect with respect to the F_1–F_1 migration path as demonstrated in figure 7(b). The three potential plots correspond to configurations where the second vacancy has almost the same distance from the centre position, but is placed at different positions of the shell of equivalent sites. The resulting values of the effective energy barriers range from 21 to 183 meV.

The thermal energy per atom at room temperature is well above the lowest barrier of 21 meV. This situation is met when the second vacancy is in forward alignment with the direction of the migration path. The effective barrier increases or remains unchanged—see figure 7(b)—if the second defect is in backward alignment with or located perpendicularly to the migrational direction, respectively. The present simple model shows that the presence of vacancies may lead to pronounced changes of the potential energies, and supports the idea that a distribution of activation energies governing the migration of F atoms is likely to occur. An improved model is, however, required to make the reasoning conclusive. We are currently applying MD techniques to study the role of defect-induced lattice relaxation and details of the migration processes.

4. Conclusions

Line-shape analysis of ^{19}F NMR allows detailed studies to be made of the heterogeneity of the ionic motion in solid electrolytes over a broad range of temperatures. The time window of the method is sensitive to dynamical effects with correlation times in the range 10^{-6}–10^{-3} s. This range can be extended to slower motions, using 2D NMR experiments, and to faster motions, using diffusion measurements combined with relaxation time measurements.

While no significant anisotropy of the motion is found in the diffusion analysis, there is clear evidence that local potentials in superionic LaF_3 have substantial spatial fluctuations. Molecular dynamics simulations show that the presence of vacancies may lead to a distribution of activation energies governing the migration of F ions. As a reason for such a distribution, local variations of the density of vacancies can be proposed. To investigate how general our model is, and to understand better the role of the potential landscape for the ionic mobility, more data from different systems with tysonite structure are now being collected and extensive simulations of ionic motion using molecular dynamics techniques are being carried out for studying the role of defect-induced lattice relaxation and details of the migration processes.

References

[1] Mahan G D W and Roth W L (ed) 1980 *Superionic Conductors* (New York: Plenum)
[2] Rössler E, Taupitz M and Vieth H-M 1990 *J. Phys. Chem.* **94** 6879
[3] Brinkmann D 1989 *Magn. Reson. Rev.* **14** 101
[4] Chung S H, Jeffrey K R, Stevens J R and Börjesson L 1990 *Solid State Ion.* **40/41** 279
[5] Walstedt R E, Dupree R, Remeika J P and Rodriguez A 1977 *Phys. Rev.* B **15** 3442
[6] Svare I, Borsa F, Torgeson D R and Martin S W 1993 *Phys. Rev.* B **48** 9336
[7] Macdonald J R 1985 *Solid State Ion.* **15** 159
[8] Schirmacher W 1988 *Solid State Ion.* **28–30** 129
[9] Funke K 1993 *Prog. Solid State Chem.* **22** 111
[10] Kim K H, Torgeson D R, Borsa F, Cho J, Martin S W and Svare I 1996 *Solid State Ion.* **91** 7
[11] Mansmann M 1965 *Z. Kristallogr.* **122** 375
[12] Maximov B and Schulz H 1985 *Acta Crystallogr.* B **41** 88
[13] Zalkin A and Templeton D H 1985 *Acta Crystallogr.* B **41** 91
[14] Privalov A F, Vieth H-M and Murin I V 1989 *J. Phys. Chem. Solids* **50** 395
[15] Sher A, Solomon R, Lee K and Muller M W 1966 *Phys. Rev.* **144** 593
[16] Ngoepe P E, Jordan W M, Catlow C R A and Comins J D 1990 *Phys. Rev.* B **41** 3815
[17] Nakamura N and Chihara H 1987 *J. Phys. Chem. Solids* **48** 833
[18] Roos A, Buijs M, Wapenaar K E D and Schoonman J 1985 *J. Phys. Chem. Solids* **46** 655
[19] Brach I and Schulz H 1985 *Solid State Ion.* **15** 135
[20] Jaroszkiewicz G A and Strange J H 1985 *J. Phys. C: Solid State Phys.* **18** 2331
[21] Roos A, van de Pol F C M, Keim R and Schoonman J 1984 *Solid State Ion.* **13** 191
[22] Belzner A, Schulz H and Heger G 1994 *Z. Kristallogr.* **209** 239
[23] Privalov A F, Vieth H-M and Murin I V 1994 *J. Phys.: Condens. Matter* **6** 8237
[24] Chang I, Fujara F, Geil B, Hinze G, Sillescu H and Tölle A 1994 *J. Non-Cryst. Solids* **172–174** 674
[25] Kaplan J I and Fraenkel G 1980 *NMR of Chemically Exchanging Systems* (New York: Academic)
[26] Press W H, Teuklosky S A, Vetterling W T and Flannery B P 1992 *Numerical Recipes in C* (Cambridge: Cambridge University)
[27] Rössler E, Kudlik A, Hess K-U, Dingwell D B, Sokolov A P and Novikov V N 1996 *Ber. Bunsenges. Phys. Chem.* **100** 1402